HHS Public Access

Author manuscript

Nat Genet. Author manuscript; available in PMC 2019 January 16.

Published in final edited form as:

Nat Genet. 2018 August ; 50(8): 1093–1101. doi:10.1038/s41588-018-0166-0.

Bi-allelic loss of human *CTNNA2*, encoding αN-catenin, leads to ARP2/3 over-activity and disordered cortical neuronal migration

Ashleigh E. Schaffer[1,2,*], **Martin W. Breuss**[1], **Ahmet Okay Caglayan**[3,4], **Nouriya Al-Sanaa**[5], **Hind Y. Al-Abdulwahed**[5], **Hande Kaymakçalan**[6], **Cahide Yılmaz**[7], **Maha S. Zaki**[8], **Rasim O. Rosti**[1], **Brett Copeland**[1], **Seung Tae Baek**[1], **Damir Musaev**[1], **Eric C. Scott**[1], **Tawfeg Ben-Omran**[9], **Ariana Kariminejad**[10], **Hulya Kayserili**[11], **Faezeh Mojahedi**[12], **Majdi Kara**[13], **Na Cai**[1], **Jennifer L. Silhavy**[1], **Seham Elsharif**[13], **Elif Fenercioglu**[14], **Bruce A. Barshop**[15], **Bulent Kara**[16], **Rengang Wang**[1], **Valentina Stanley**[1], **Kiely N. James**[1], **Rahul Nachnani**[1], **Aneesha Kalur**[2], **Hisham Megahed**[8], **Faruk Incecik**[17], **Sumita Danda**[18], **Yasemin Alanay**[19], **Eissa Faqeih**[20], **Gia Melikishvili**[21], **Lobna Mansour**[22], **Ian Miller**[23], **Biayna Sukhudyan**[24], **Jamel Chelly**[25], **William B. Dobyns**[26], **Kaya Bilguvar**[3], **Rami Abou Jamra**[27], **Murat Gunel**[3], and **Joseph G. Gleeson**[1,*]

[1]Department of Neuroscience, Rady Children's Institute for Genomic Medicine, Howard Hughes Medical Institute, University of California, San Diego, CA, USA

[2]Department of Genetics and Genome Sciences, Case Western Reserve University, Cleveland, OH, USA

[3]Yale Program on Neurogenetics, Departments of Neurosurgery, Neurobiology, and Genetics, Yale University School of Medicine, New Haven, CT, USA

[4]Department of Medical Genetics, Istanbul Bilim University, Istanbul, Turkey

[5]Department of Pediatrics, Johns Hopkins Aramco Healthcare, Dhahran, Kingdom of Saudi Arabia

[6]Department of Pediatrics, Istanbul Bilim University, Istanbul, Turkey

[7]Department of Pediatrics, Yıldırım Beyazıt University, Ankara, Turkey

*Addressed correspondence to: jogleeson@ucsd.edu or ashleigh.schaffer@case.edu.

URLs

NHLBI Exome Sequencing Project (ESP) http://evs.gs.washington.edu/EVS/
SeattleSeq http://snp.gs.washington.edu/SeattleSeqAnnotation137/
OMIM http://www.omim.org/
PolyPhen-2 http://genetics.bwh.harvard.edu/pph2/
NCBI Gene *CTNNA2*: https://www.ncbi.nlm.nih.gov/gene/1496

Author Contributions

N.A-S., H.Y.A-A., H.K., C.Y., R.O.R., V.S., K.N.J., M.S.Z., S.E., T. B-O., A. Karminejad, H. Kayserili, F.M., M.K., E. Fenercioglu, B.K., H.M., F.I., S.D., Y.A., E. Faqeih, G.M., B.A.B. L.M., I.M., B.S., J.C., W.B.D., M.G. and J.G.G. performed patient recruitment and phenotyping. A.E.S. A.O.C., S.T.B., B.C., D.M., E.C.S., K.B., J.L.S., M.G., and J.G.G. supported sequencing and variant interpretation. A.E.S., N.C., R.W., and R.N. performed the tissue culture experiments. A.E.S. and A. Kalur. generated recombinant proteins and performed the actin assays. A.E.S., M.B. and J.G.G. wrote the manuscript. A.E.S., M.B., and J.G.G. edited the manuscript, and J.G.G. directed the project.

[8]Clinical Genetics Department, Human Genetics and Genome Research Division, National Research Centre, Cairo, Egypt

[9]Clinical and Metabolic Genetics Section, Department of Pediatrics, Hamad Medical Corporation, Doha, Qatar

[10]Kariminejad-Najmabadi Pathology and Genetic Center, Tehran, Iran

[11]Department of Medical Genetics, Koç University School of Medicine, Topkapı, Istanbul, Turkey

[12]Mashhad Medical Genetic Counseling Center, Mashhad, Iran

[13]University of Tripoli, Tripoli Children's Hospital, Tripoli, Libya

[14]L.E.S. Mikrogen Genetic Diseases Diagnosis Center, Istanbul, Turkey

[15]Department of Pediatrics, Biochemical Genetics Program, University of California, San Diego, CA, USA

[16]Kocaeli University, Department of Pediatric Neurology, Umuttepe, Kocaeli, Turkey

[17]Cukurova University, Department of Pediatric Neurology, Adana, Turkey

[18]Department of Clinical Genetics, Christian Medical College and Hospital, Vellore, Tamil Nadu, India

[19]Pediatric Genetics Unit, Department of Pediatrics, Acibadem Mehmet Ali Aydinlar University, Istanbul, Turkey

[20]Section of Medical Genetics, Department of Pediatrics, King Fahad Medical City, Children's Hospital, Riyadh, Kingdom of Saudi Arabia

[21]Department of Pediatrics, MediClubGeorgia, Tbilisi, Georgia

[22]Pediatric Department, Neuropediatric Unit, Cairo University Children's Hospital, Cairo, Egypt

[23]Neurology Department, Nicklaus Children's Hospital, Miami, FL, USA

[24]Arabkir Joint Medical Center & Institute of Child and Adolescent Health, Yerevan, Armenia

[25]Institut Cochin, Université Paris-Descartes, CNRS (UMR 8104), Paris, France

[26]Departments of Pediatrics and Neurology, University of Washington and Center for Integrative Brain Research, Seattle Children's Research Institute, Seattle, WA, USA

[27]Institute of Human Genetics, University of Leipzig Hospitals and Clinics, Leipzig, Germany

Abstract

Neuronal migration defects, including pachygyria, are among the most severe developmental brain defects in humans. Here we identify bi-allelic truncating mutations in *CTNNA2,* encoding αN-catenin, in patients with a distinct recessive form of pachygyria. *CTNNA2* was expressed in human cerebral cortex, and its loss in neurons led to defects in neurite stability and migration. The αN-catenin paralog, αE-catenin, acts as a switch regulating the balance between α-catenin and Arp2/3 actin filament activities[1]. Loss of αN-catenin did not affect β-catenin signaling, but recombinant αN-catenin interacted with purified actin and repressed ARP2/3 actin-branching

activity. The actin-binding domain (ABD) of αN-catenin or ARP2/3 inhibitors rescued the neuronal phenotype associated with *CTNNA2* loss, suggesting ARP2/3 de-repression as a potential disease mechanism. Our findings identify *CTNNA2* as the first catenin family member with bi-allelic mutations in human, causing a new pachygyria syndrome linked to actin regulation, and uncover a key factor involved in ARP2/3 repression in neurons.

Keywords

alpha-catenin; actin remodeling; Arp2/3; neuronal migration; centrosome; pachygyria; polarity; primary neurite; Wnt signaling; beta-catenin

---

The Lissencephaly (LIS) spectrum is characterized by defects in the folding pattern of the cerebral cortex, resulting in reduced number or complexity of gyri that characterize the human brain[2]. LIS encompasses a continuum of malformations ranging from complete agyria to pachygyria, in which gyral formation is diminished but not absent. Patients present clinically with failed motor and cognitive development followed by intractable epilepsy. Most patients are severely intellectually impaired, and are unable to walk or care for themselves.

Projection neurons of the cerebral cortex are born in a zone adjacent to the ventricle, and then migrate to the future six-layered neocortex. Neuronal migration is achieved through a rearrangement of cytoskeletal components in response to extracellular cues, mediated by numerous intracellular signaling pathways[3]. Coordinated regulation of monomeric (G-actin) and polymerized actin microfilaments (F-actin) is critical for neuronal growth cone morphogenesis, axon pathfinding, and neurite extension during migration[4,5]. Positive regulators of F-actin assembly include families of nucleating proteins (Formins, Arp2/3) and their co-activators (Rho GTPases, WASP, WAVE), but negative regulators remain elusive, particularly in neurons[6].

We recruited three families, with seven affected individuals showing neurodevelopmental delay (Fig. 1a, Table 1). All were diagnosed before age two years and displayed acquired microcephaly, hypotonic cerebral palsy, inability to ambulate or speak, and intractable seizures. (Table 1). Magnetic resonance imaging (MRI) demonstrated pachygyria with dramatic cortical gray matter thickening up to 3–4 cm, with paucity of gyri without obvious posterior-anterior gradient or focal dysplasias. There was absent anterior commissure, hypogenesis of the corpus callosum, and cerebellar hypoplasia (Fig. 1b). This phenotype is distinct from *LIS1*-pachygyria or *DCX*-pachygyria, which show posterior- or anterior-gradients, respectively. All subjects were enrolled in institutional review board (IRB) approved protocols and provided consent for study. We performed whole exome sequencing[7] on at least one member of each family[8]. We prioritized rare (<0.2% allele frequency) damaging variants (GERP score >4 or SIFT <0.05), and focused on homozygous variants due to parental consanguinity. Parametric linkage analysis from genome-wide SNP arrays and homozygosity mapping[9,10] showed identical-by-descent haplotypes (Supplementary Fig. 1a). Aligning variants with corresponding homozygous intervals identified putative nonsense variants in *CTNNA2* in all three families (Family 1101, c.2664C>T p.Arg882*; Family 1263, c.2341C>T p.Arg781*; Family 4727, c.1480C>T p.Arg494*) (Fig 1c, d,

Supplementary Fig. 1b). The three variants were each observed only heterozygous once in the public databases ExAC and gnomAD. Sanger sequencing confirmed segregation according to a strict recessive mode of inheritance, with full penetrance, in all genetically informative available family members, suggesting that bi-allelic *CTNNA2* loss-of-function mutations underlie pachygyria in these patients.

CTNNA2 is the ancestral α-catenin gene and is conserved in all Metazoa, but is predominantly expressed in brain in mammals[11]. *CTNNA1* is the most widely expressed, but is absent from populations of migrating neurons[12], whereas *CTNNA3* is expressed predominantly in myocardium. We confirmed *CTNNA2* expression in human neural tissue (Supplementary Fig. 2a), and found protein co-expression with migration markers Dcx and Tuj1 in murine embryonic day (e) 13.5 brain (Supplementary Fig. 2b). As reported in mouse, a rim of αN-catenin was expressed in the apically localized progenitors of the ventricular zone[12]. In 20-week gestation human fetal brain αN-catenin was mostly restricted to regions expressing DCX and TUJ1 in developing cortical plate and marginal zone (Supplementary Fig. 2c).

There are two mouse lines harboring loss-of-function mutations of the ortholog to human *CTNNA2* (*Catna2*). *Cerebellar deficient folia (cdf)* mice have a spontaneous C-terminal deletion[13–15], and the conventional knockout removed the first exon[16]. These mutants share multiple phenotypes including impaired lamination of a subset of Purkinje and hippocampal neurons[13–16], hippocampal dendritic spine morphogenesis[16,17], axon projections, positioning of subsets of nuclei-specific neurons, and midline axonal crossing[18]. Of note, many of the phenotypes present in *Catna2* mice are shared with *CTNNA2* patients, including cerebellar hypoplasia and midline defects, however, neither line showed evidence of an overt neocortical phenotype[15]. This was not surprising given that mouse models for human cortical migration defects typically show no neocortical defects.

In order to investigate migration in a human model, we generated iPSC and neuronal derivatives from the affected and unaffected member of Family 1263 (1263A and Control, respectively), an individual with LIS due to Miller-Dieker syndrome (MDS, deletion of chromosome 17p11.3) as well as targeted the *CTNNA2* gene in the H9 hESC line (herein referred to as $CTNNA2^{KO}$) [19] (Supplementary Fig. 3). Western blot of the neuronal progenitor cells (NPCs) demonstrated absent αN-catenin protein in the patient and knockout compared to Control (Supplementary Fig. 4).

To study migration, we adopted a neurosphere assay[20], and measured neuronal cell body distances from the edge after 48 hrs. We first confirmed cells exiting the neurosphere expressed postmitotic neuronal markers and were negative for other lineages (Supplementary Fig. 5a, b). GFAP-positive cells were only observed at the edge of the plated spheres in all of the lines tested (Supplementary Fig. 5a, b). Cell bodies of Control neurons showed a migration front at 514 μm (Fig. 2a, ave. 115 μm, S.D. 97 μm), whereas MDS (ave. 31 μm, S.D. 22 μm, P = 3.28E-34), *CTNNA2* patients (ave. 33 μm, S.D. 21 μm, P = 1.19E-27), and $CTNNA2^{KO}$ (ave. 36 μm, S.D. 22 μm, P = 1.01E-18) lines were less than half normal. Consistent with what has been observed in MDS and control cerebral organoid models of neuronal migration[21], the distribution of distances of MDS, *CTNNA2* patient, and

CTNNA2^{KO} exited-neurons was significantly reduced (Fig. 2a, Supplementary Fig. 6, Supplementary Fig. 7). We conclude that loss of *CTNNA2* results in a neuronal migration defect *in vitro*.

Time-lapse phase microscopy was performed to study the mechanism of defective migration. Control cells displayed bipolar morphology, with leading neurite length on average 130 μm. *CTNNA2*-mutant cells showed shortened (ave. length 18 μm) disorganized leading processes, enlarged growth cones, proximal ectopic filopodia and lamellipodia, and failed bipolar morphology (Fig. 2b, Supplementary Movie 1–3). We confirmed that the neurite length and migration defect were due to absence of *CTNNA2* using lentiviral transduction rescue with GFP-tagged *CTNNA2.* Transduced cells had uniform expression of a full-length αN-catenin-GFP at 129 kDa and a processed product at 102 kDa (Supplementary Fig. 8a). Neurite length and migration were largely restored in both patient and *CTNNA2*^{KO} cells upon *CTNNA2*-GFP forced-expression (Fig. 2b, c, Supplementary Fig. 6, Supplementary Fig. 7).

Previous studies have shown mouse αE-catenin, encoded by *Catna1,* is required for preimplantation epithelial integrity[22], whereas conditional deletion in embryonic brain disrupts adherens junctions, leading to dysregulated proliferation[23]. To test whether loss of *CTNNA2* affects neuroepithelium polarity, we generated neural rosettes from Control and 1263A iPSCs and used immunostaining to examine apical polarization. Despite the absence of αN-catenin at the apical surface of the rosette, the tight junction marker ZO-1 and the adherens junction markers N-Cadherin and β-Catenin were localized in a polarized fashion near cilia (Supplementary Fig. 9). These results suggest loss of *CTNNA2* does not adversely affect apical polarization of neuroepithelial cells in culture.

The presence of a putative β-catenin binding domain suggests αN-catenin loss may alter Wnt signaling[24]. We therefore compared gene expression profiles between MDS, 1263A and Control NPCs by RNA-sequencing. We found no consistent, differential expression changes, arguing against a major transcriptional effect (Supplementary Fig. 10 a–c). Furthermore, established canonical Wnt target genes were not changed (Supplementary Fig. 10d), suggesting loss of *CTNNA2* does not measurably impact Wnt-mediated transcription.

We thus focused on potential αN-catenin regulation of the neuronal cytoskeleton. αN-catenin contains a putative F-actin binding domain (ABD) at the C-terminus. To assess the ability of αN-catenin to directly bind and bundle actin, we performed actin binding and bundling assays *in vitro.* Similar to the α-actinin control, full-length recombinant αN-catenin co-sedimented with F-actin (Fig. 3a, Supplementary Fig. 11). Full-length αN-catenin appeared to weakly bundle F-actin filaments (Fig. 3b), although more work would be necessary to assess direct bundling activity. There was no noticeable change in the G-actin/F-actin ratio in NPCs from control or affected (Supplementary Fig. 12), arguing against an overall effect on actin stabilization.

We next generated lentiviral constructs lacking or containing amino acids 671–905, corresponding to the αN-catenin ABD[25], and confirmed that encoded protein was stable in NPCs (Supplementary Fig. 8b, c). *CTNNA2*$^{\Delta ABD}$ could not rescue migration defects in the

CTNNA2^{KO} neurons, and had no effect on Control cells (Fig. 3c, Supplementary Fig. 6, 7). In contrast, expression of *CTNNA2*^{ABD} alone mediated rescue of migration in *CTNNA2*^{KO}, and enhanced migration in Control neurons (Fig. 3c, Supplementary Fig. 6, 7). We conclude the ABD of *CTNNA2* is necessary and sufficient for its effect on neuronal migration in *CTNNA2*-mutant cells.

The reduction in leading process stability we observed in *CTNNA2*-mutant neurons was similar to a phenotype recently described in mouse *Arpc2* mutant radial glia[26], suggesting αN-catenin might regulate Arp2/3 activities. Recombinant αE-catenin controls actin-filament organization and represses Arp2/3-mediated actin polymerization *in vitro*[25]. Thus, we reasoned that the excessive filopodia formation, accompanied by repeated, rapid retraction of the leading process in *CTNNA2*-mutant neurons, might result from failure to suppress ARP2/3-mediated actin branching. To initiate actin branching, the ARP2/3 complex binds to the side of existing F-actin filaments to nucleate a new filament at a distinctive 70° angle; and consequently ARP2 and ARP3 are incorporated into the microfilament structure[27]. To test for increased F-actin branching, we assessed the amount of ARP3 protein associated with F-actin filaments. Migrating neurons from the MDS patient showed ARP3 associated with actin to be equal to or less than Control, whereas neurons from 1263A and *CTNNA2*^{KO} lines showed almost a 50% increase in association (Fig. 4a, c, Supplementary Fig. 13a, b). We conclude that *CTNNA2*-deficient cells show excessive association between ARP2/3 and actin.

ARP2/3 initiates actin branching in the presence of the Wiskott-Aldrich syndrome family protein (WASP) VCA domain by the nucleation of F-actin filaments. We thus tested whether αN-catenin was sufficient to inhibit the effect of ARP2/3 + VCA on actin polymerization. Recombinant VCA domain of human WASP (400 nM) showed minimal actin polymerizing activity. This was more than doubled upon addition of 10 nM ARP2/3 complex. Increasing concentrations of recombinant αN-catenin resulted in a dosage-dependent inhibition on the ARP2/3 + VCA effect on actin, reduced nearly back to baseline (Fig. 4b). We conclude that αN-catenin is sufficient to suppress the effect of ARP2/3 + VCA on actin polymerization *in vitro*.

Since αN-catenin repressed ARP2/3 activity *in vitro*, we next tested whether this activity was mediated by the ABD using *CTNNA2*^{KO} neurons. We ectopically expressed αN-catenin ABD and assessed the amount of ARP3 associated with actin by Western blot. We observed a near doubling of ARP3 associated with F-actin, whereas expressing the αN-catenin ABD showed potent loss of most ARP3 bound to actin (Fig. 4c, Supplementary Fig. 13b), suggesting the ABD domain of αN-catenin is sufficient to regulate ARP2/3 – actin interaction. We also tested the ability of recombinant αN-catenin ABD to repress ARP2/3-mediated actin polymerization *in vitro*. The ABD of αN-catenin was sufficient to repress ARP2/3 mediated actin polymerization in a dosage-dependent manner (Supplementary Fig. 13c), albeit to a lesser extent than full-length αN-catenin.

If αN-catenin mediates its effects on neuronal morphology through suppression of ARP2/3, then inhibition of ARP2/3 should at least partially compensate for the loss of αN-catenin in neurons. To test this, we used two different cell-permeable ARP2/3 inhibitors, CK-666 or

CK-869[28], which inhibit ARP2/3 at different sites. After generating a dose-response curve, we analyzed neurite length in Control, MDS, patient, and *CTNNA2*^{KO} migrating neurons after 24 hrs. A majority of Control neurons showed long, extended bipolar neurites with ave. length > 100 μm. Both inhibitors showed a negative effect on neurite length in Control neurons, but *CTNNA2*-mutant cells increased neurite length nearly 10-fold, restoring the distribution to near Control levels (Fig. 4d, Supplementary Fig. 7, 14). MDS neurons showed neurites on average 18 μm in length, without improvement upon ARP2/3 inhibitor treatment. We conclude that ARP2/3 inhibitors can largely rescue the neurite length defect associated with loss of *CTNNA2*.

In summary, we have identified a new neuronal migration disorder due to bi-allelic truncating mutations in *CTNNA2*. The involvement of an actin regulator in pachygyria was surprising, given that previously genetic studies focus on microtubules[29]. Microtubules scaffold the cytoskeleton for the repeated cycles of migration[30,31]. The main effect of actin appears to be in sensing and responding to extracellular guidance cues through changes in cell morphology, as well as guiding microtubules within the primary neurite[32]. This is mediated at least in part by calcium influx and enhanced neuronal motility through LIS1-dependent regulation of Rho GTPases[33], but also through transmembrane proteins, which can alter cell morphology through effects on actin[34].

Actin structure is critically regulated by Arp2/3, which controls the decision to initiate branching. We show Arp2/3 over-activity, as a result of loss of αN-catenin, leads to excessive branching, which impairs neurite growth and stability, possibly by controlling microtubule advance into the growth cone[32,35]. αN-catenin suppresses actin branching; *in vivo* this likely occurs by binding F-actin. This activity is mediated by the ABD, which we show competes with ARP2/3 for nucleation sites on F-actin. α-actinin, fascin and αE-catenin can sort actin associated proteins by altering the conformation of actin[1,25,36]. It will be interesting to determine if αN-catenin also shares this property or if it extends to other ABD containing proteins. Thus, as a more general principle, actin-binding proteins may serve unrecognized roles in actin regulation by controlling F-actin polymerization as well as dictating actin conformation locally within a cell.

Online Methods

Please see the accompanying Life Sciences Reporting Summary for further detailed explanation of experimental design and analysis used in this study.

Patient Recruitment

Patients were enrolled and sampled according to standard local practice in approved human subjects protocols at the respective institutions. Each subject was evaluated by and had MRI images by one of the authors. Excluded were cases with overlapping conditions such as asymmetrical brain dysplasia, primary white matter disease, or evidence of altered metabolism such as elevations in lactate or abnormal peaks on standard clinical serum tandem mass spectroscopy.

Exome Sequencing

For each sample, DNA was extracted from peripheral blood leukocytes by salt extraction. Exon capture was performed with the Agilent SureSelect Human All Exome 50 Mb Kit with paired-end sequencing on an Illumina HiSeq2000 instrument resulting in >94% recovery at > 10x coverage.

Sequences were aligned to the human genome (hg19) with Burrows-Wheeler Aligner (BWA) and variants delineated using the Genome Analysis Toolkit (GATK) software and SAMTools algorithms for both SNPs and insertion/deletion polymorphisms[8]. Variants were filtered for the criteria: 1] occurring in coding regions and/or splice sites, 2] non-synonymous, 3] found in less than 0.1% frequency in control populations (our in house exome data set of 12,000 individuals, dbSNP and Exome variant server) 4] homozygous in consanguineous families, 5] within linkage intervals or blocks of homozygosity. Variants were ranked by the type of mutation (nonsense/splice/indel > missense), amino acid conservation across species, and damage prediction programs (PolyPhen and Grantham score).

Linkage Analysis

All informative members of Family-1101 were genotyped with the Infinium iSelect24 mapping panel (Center for Inherited Disease Research) and analyzed with easyLINKAGE-Plus software[37]. Parameters were autosomal recessive with full penetrance and disease allele frequency of 0.001. Genomic regions with LOD scores under -2 were excluded as loci, over 2 were considered as candidate loci, and over 3.3 as statistical evidence for genome-wide significance. Linkage simulations were performed with Allegro 1.2c under the same parameters, with 5,000 markers at average 0.64 cM intervals, codominant allele frequencies, and parametric calculations[37].

Tissue Culture

Fibroblasts were generated from unaffected and affected dermal biopsies explants and cultured in MEM (Gibco), supplemented with 20% FBS (Gemini). iPSCs, neural progenitor cells and neurons were obtained as previously described[19,38]. MDS fibroblasts were obtained from Coriell Biorepository (GM09209) and similarly reprogrammed.

iPSCs were generated as previously described[39] using 3 μg expression plasmid mixtures (OCT3/4, SOX2, KLF4, L-MYC, LIN28 and p53 shRNA) electroporated into $6x10^5$ cells, dissociated after 7 d, and $1.5x10^5$ cells re-plated onto 100 mm dishes with $1.5x10^5$ irradiated CF-1 mouse embryonic fibroblasts (MEF) feeder layer. Culture medium was replaced every day with hESC/iPSC medium (DMEM:F12 supplemented with 20% KOSR and 20 ng/ml bFGF (Invitrogen), 1x non-essential amino acids, 110 mM 2-mercaptoethanol. Colonies with healthy appearance (rounded smooth edges) were selected for further cultivation and evaluation. After 3 passages iPSCs cells were transferred to Matrigel (BD Biosciences) coated plates and grown in mTeSR medium (Stem Cell Technologies).

Neural progenitors cells (NPCs) were obtained as previously described[40] with embryoid bodies (EBs) formed by mechanical dissociation of cell clusters and plated in suspension in

differentiation medium (DMEM:F12, 1x N2, 1 μM Dorsomorphin (Tocris), 2 μM A8301 (Tocris)) and kept shaking at 95 rpm for 7 days, then plated onto Matrigel (BD Biosciences) coated dishes in NPC medium (DMEM:F12, 0.5x N2, 0.5x B27, 20 ng/ml bFGF). Rosettes were visible after 5–7 d, selected with Neural Rosette Selection Media (StemCell Technologies), and NPCs plated onto poly-L-ornithine (PLO)/laminin (Sigma) dishes with NPC medium, which was exchanged every 2 days.

Bright field images were taken on Axiovert.A1, or AxioObserver inverted microscopes (Zeiss), in addition to an EVOS microscope (Life Technologies) and processed with Photoshop CS5 (Adobe Systems). Time-lapse movies were acquired on a Zeiss Axio Observer and compiled with Zeiss Zen software. Fluorescent confocal images of neural rosettes were taken on an LSM 880 (Zeiss) and processed with FIJI/ImageJ software. Images are maximum z-projections of the entire depth of signal for the cell of interest.

CRISPR Targeting

Frame-shifting insertions or deletions (indels), occurring in coding exon 12 of *CTNNA2,* were generated in H9 hESCs by CRISPR/SpCas9 induced imprecise non-homologous end joining (NHEJ) as previously described[41] with CTNNA2 sgRNA-F and CTNNA2 sgRNA-R primers (Supplementary Table 1) into BbsI-digested px330. Individual colonies were isolated after 2 wks, expanded, and genotyped by Sanger sequencing for bi-allelic mutations.

cDNA synthesis and RT-PCR

cDNA synthesis of 1 μg patient RNA was performed with Superscript III First-Strand RT-PCR (Life Technologies). The reaction products were then used for quantitative real-time PCR (qRT-PCR) or cloning. qRT-PCR was performed in triplicate on 10 ng human cDNA for *CTNNA2*, *AXIN2*, *ID2*, *LEF1*, and *GAPDH* (see Supplementary Table 1 for primer sequences). CT values were normalized to GAPDH as a loading control and fold change calculated in reference.

Neurosphere Assays

Neurosphere assay methods were modified from previously described protocols[42]. Three different stem cell lines (clones) per patient or condition were used as biological replicates for each experiment. The iPSC-derived NPCs were dissociated and incubated, shaking at 95 RPM, in NPC media. The following day, the media was changed to DMEM:F12 with 1x N2, 1x B27, shaking at 95 RPM for 12 hrs, the resultant neurospheres plated on PLO/laminin plates, and imaged at 48 hrs to record distance each neuronal cell body traveled from the edge of the neurosphere using FIJI/ImageJ (NIH) per clone. Data from each clone was collected and analyzed together with data from the other 2 clones per patient or condition to facilitate statistical tests.

Neurite Quantification

Three different stem cell lines (clones) per patient or condition were used as biological replicates for each experiment. To assess leading process length, stem cell derived migrating neurons were imaged. The length of the primary neurite from the edge of the cell body to the tip of the growth cone was measured in microns. For ARP2/3 inhibition, 0.2 μM CK-666,

0.2 μM CK-869, or an equivalent dilution of DMSO was added to the neurons 6 hrs after plating[28]. Neurons were analyzed after 24 hr. Data from each clone was collected and analyzed together with data from the other 2 clones per patient or condition to facilitate statistical tests.

RNA sequencing

Total RNA was extracted from two NPC lines per patient with TRIzol Reagent (Gibco). Full length mRNA was captured by TruSeq Stranded mRNA kit (Illumina) with standard protocol and was submitted for paired-end 100 nucleotide sequencing on MiSeq (Illumina). Roughly 30 million reads per sample were aligned to the 1000 Genomes Project's version of GRCh37 using standard TopHat2 (http://ccb.jhu.edu/software/tophat/) v2.0.11 with paired-end read options and allowing for intron-spanning reads as defined by transcripts in Illumina iGenomes NCBI build 37.2. The pairwise euclidean distance between all samples using the filtered (median FPKM>1) and log2 transformed gene expression values was calculated, and Pearson's correlation determined. Differential expression on a gene-based level was tested for with cuffdiff 59 v2.1.1 using default option. Genes reported as significantly differentially expressed between a pair of conditions were determined to have been so based on cuffdiff threshold of a 0.05 false-discovery rate corrected *p*-value.

Histology

Animal use followed NIH guidelines and was approved by IACUC at UCSD and Rockefeller University. *Wild type* mice (C57BL/6N) were obtained from Jax and intercrossed to produce embryonic day (e) 13.5 embryos. The embryos were fixed in 4% PFA, cryoprotected then sectioned. Human fetal brain was obtained from the UCSD autopsy service, fixed in 4% PFA and embedded in paraffin. Microtome sections were deparaffinized, blocked with 4% donkey serum, incubated in primary antibody overnight, washed, incubated in secondary antibody for 1 hr, post-fixed in 4% PFA, and counterstained with DAPI or Nissl for imaging.

αN-catenin Lentivirus

Full-length, the actin binding domain (ABD, amino acids 671–905), or the actin binding domain deleted (ΔABD, amino acids 1–670) αN-catenin was cloned into pLVX-AcGFP-N1 vector (Clontech) and co-transfected with psPAX2 and pCMV-VSVg (Addgene) into Lenti-X 293T cells (Clontech) to generate lentivirus. Virus containing media was collected at 66 hrs, concentrated by ultracentrifuge, and stored at −80°C. Patient-derived NPCs were transduced with lentivirus and selected with 1 μg/ml puromycin for 48 hrs before proceeding with experiments.

Recombinant αN-catenin Protein Generation

cDNA encoding full-length αN-catenin was amplified and cloned into bacterial GST expression vector pGEX-6P-1 (GE Healthcare Life Sciences). Recombinant αN-catenin was produced in BL21 cells and affinity purified with anti-GST MagneGST beads (Promega).

Actin Assays

Actin binding and bundling assays were performed according to manufacturer's recommendations (Cytoskeleton, Inc., BK001). Actin polymerization assays were performed with pyrene actin (Cytoskeleton, Inc., AP05), α-actinin, GST-tagged VCA domain of human WASP protein (#VCG03), and Arp2/3 protein complex from porcine brain (Cytoskeleton, Inc., RP01P) according to manufacturer's recommendations, with the addition of recombinant αN-catenin. G:F Actin ratios were determined in triplicate from patient-derived NPCs using G-Actin/F-Actin In Vivo Assay Biochem Kit (Cytoskeleton, Inc., BK037). CK-666 and CK-869, block an activating conformational change, binding to different sites[28]. CK-666 stabilizes the inactive state of the complex, blocking movement of the Arp2 and Arp3 subunits into the activated filament-like (short pitch) conformation, while CK-869 binds to a serendipitous pocket on Arp3 and allosterically destabilizes the short pitch Arp3-Arp2 interface.

F-actin Pulldown

Phalloidin-mediated F-actin pulldown was performed as described[43] with Biotin-XX phalloidin (Life Technologies, B7474) then streptavidin conjugated magnetic beads (Pierce Protein Biology), washed 3x, then boiled.

Antibodies

Primary antibodies used for immunocytochemistry or Western blot include mouse anti-GAPDH (Millipore), mouse anti-Nestin (Millipore), mouse anti-Tuj1/βIII-tubulin (Millipore), mouse anti-Tuj1/βIII-tubulin (Santa Cruz Biotenchnology), mouse anti-TRA-1-60 (Millipore), mouse anti-TRA-1-81 (Millipore), goat anti-Lin28a (R&D Systems), rabbit anti-Nanog (Santa Cruz Biotechnology), rabbit anti-Oct3/4 (Santa Cruz Biotechnology), rabbit anti-DCX[44], goat anti-DCX (Santa Cruz Biotechnology), goat anti-SOX2 (Santa Cruz Biotechnology), rabbit anti-PAX6 (Covance), mouse anti-MAP2 (Millipore), mouse anti-BLBP (Abcam), rabbit anti-GFAP (Sigma), rabbit anti-OLIG2 (Abcam), mouse anti-β-Catenin (BD), rabbit anti-Arp3 (Santa Cruz Biotechnology), mouse anti-β-actin (Sigma), rabbit anti-EIF3D (Bethyl Labs), rat anti-αN-catenin obtained from the NIH NICHD Developmental Studies Hybridoma Bank (Catalog: NCAT2, deposited by Masatoshi Takeichi and Shinji Hirano). Fluorophore conjugated secondary antibodies were purchased from Invitrogen, and immunohistochemistry was performed with ABC Elite peroxidase staining kit, using ImmpactDAB as a substrate.

Statistics

Neuronal migration and neurite length was graphed in MS Excel as a box plot with quartile 1, median, and quartile 3 displayed. Whiskers represent the maximum and minimum observed values for each comparison group across all replicates. Western blot densitometry and fold change gene expression was plotted as a bar graph with the average of at least 3 replicates displayed, or the values displayed on the figure. Error bars represent the standard error of the mean. Unpaired, 2-tailed student's *t* test was used to calculate significance (* $P<0.05$, ** $P<0.001$, *** $P<0.0001$, n.s. not significant.) Fig. 2a: Control vs MDS, $P = 3.29\text{x}10^{-34}$; Control vs 1263A, $P = 1.20\text{x}10^{-27}$; Control vs CTNNA2^{KO}, $P = 1.01\text{x}10^{-18}$.

Fig. 2b: Control vs 1263A, $P = 2.74x10^{-26}$; Control vs CTNNA2^{KO}, $P = 4.03x10^{-57}$; Control vs Control + *CTNNA-GFP*, $P = 2.64x10^{-7}$; 1263A vs 1263A + *CTNNA-GFP*, $P = 4.30x10^{-26}$; CTNNA2^{KO} vs CTNNA2^{KO} + *CTNNA-GFP*, $P = 1.66x10^{-59}$; Control vs 1263A + *CTNNA-GFP*, $P = 0.04$; Control vs CTNNA2^{KO} + *CTNNA-GFP*, $P = 0.73$. Fig. 3c: Control vs Control + *CTNNA-GFP*, $P = 0.29$; CTNNA2^{KO} vs CTNNA2^{KO} + *CTNNA-GFP*, $P = 1.15x10^{-21}$; Control vs CTNNA2^{KO} + *CTNNA-GFP*, $P = 0.10$. Fig. 3c: Control vs Control + *CTNNA*$^{\Delta ABD}$, $P = 0.65$; Control vs Control + *CTNNA*^{ABD}, $P = 2.68x10^{-21}$; CTNNA2^{KO} vs CTNNA2^{KO} + *CTNNA*$^{\Delta ABD}$, $P = 0.06$; CTNNA2^{KO} vs CTNNA2^{KO} + *CTNNA*^{ABD}, $P = 1.81x10^{-30}$. Fig. 4c: Control vs Control + CK-666, $P = 3.37x10^{-3}$; MDS vs MDS + CK-666, $P = 0.29$; 1263A vs 1263A + CK-666, $P = 5.75x10^{-19}$; CTNNA2^{KO} vs CTNNA2^{KO} + CK-666, $P = 3.48x10^{-52}$; Control vs MDS + CK-666, $P = 2.12x10^{-53}$; Control vs 1263A + CK-666, $P = 0.03$; Control vs CTNNA2^{KO} + CK-666, $P = 4.86x10^{-10}$. Supplementary Fig. 4: Control vs 1263A, $P = 0.003$; no detectable protein in CTNNA2^{KO}. Supplementary Fig. 8: *AXIN2* Control vs 1263A, $P = 0.81$; *ID2* Control vs 1263A, $P = 0.53$; *LEF1* Control vs 1263A, $P = 0.32$. Supplementary Fig. 10: Control vs 1263A, $P = 0.35$. Supplementary Fig. 11: Control vs Control + CK-869, $P = 1.88x10^{-17}$; MDS vs MDS + CK-869, $P = 2.47x10^{-5}$; 1263A vs 1263A + CK-869, $P = 1.18x10^{-38}$; CTNNA2^{KO} vs CTNNA2^{KO} + CK-869, $P = 5.47x10^{-57}$; Control vs MDS + CK-869, $P = 1.47x10^{-61}$; Control vs 1263A + CK-869, $P = 5.22x10^{-6}$; Control vs CTNNA2^{KO} + CK-666, $P = 0.26$.

Data Availability

The datasets generated and analyzed for the current study are have been deposited in the database Genotypes and Phenotypes (dbGaP) with accession numbers phs000288 and phs000744 and the Gene Expression Omnibus (GEO) repository with accession number GSE72994.

Supplementary Material

Refer to Web version on PubMed Central for supplementary material.

Acknowledgments

We thank the patients and their families for participation. We thank A. Wynshaw-Boris for his generous scientific and editorial input. The research was supported by NIH R01NS041537, R01NS048453, R01NS052455, P01HD070494, P30NS047101, Qatar National Research Fund (QNRF) # 6-1463-351, the Simons Foundation Autism Research Initiative (SFARI), and the Howard Hughes Medical Institute (J.G. Gleeson). A.E. Schaffer is a recipient of an A.P. Gianinni Fellowship and an NIH Pathway to Independence Award, R00HD082337. S.T. Baek is supported by a 2014 NARSAD Young Investigator Grant from the Brain & Behavior Research Foundation. We thank the Broad Institute and, the Yale Center for Mendelian Disorders (UMIHG008900 to D. MacArthur and H. Rehm, and UMIHG006504 to R. Lifton and M. Gunel), and the Gregory M. Kiez and Mehmet Kutman Foundation to M.Gunel. We acknowledge M. Gerstein, S. Mane, A. B. Ekici, ad S. Uebe for sequencing support and analysis, the Yale Biomedical High Performance Computing Center for data analysis and storage, the Yale Program on Neurogenetics, and the Yale Center for Human Genetics and Genomics. Exome data has been deposited into dbGaP (phs000288). The authors declare no competing financial interests.

Abbreviations

CTNNA2	Alpha-N-catenin
LIS1 or PAFAH1B1	lissencephaly-1

DCX	doublecortin
MDS	Miller Dieker syndrome
iPSC	induced pluripotent stem cell
NPC	neural progenitor cell
ABD	actin-binding domain

References

1. Drees F, Pokutta S, Yamada S, Nelson WJ, Weis WI. α-Catenin is a molecular switch that binds E-Cadherin-β-Catenin and regulates actin-filament assembly. Cell. 2005; 123:903–915. [PubMed: 16325583]
2. Leventer RJ, Guerrini R, Dobyns WB. Malformations of cortical development and epilepsy. Dialogues Clin Neurosci. 2008; 10:47–62. [PubMed: 18472484]
3. Ayala R, Shu T, Tsai LH. Trekking across the brain: the journey of neuronal migration. Cell. 2007; 128:29–43. [PubMed: 17218253]
4. Meyer G, Feldman EL. Signaling mechanisms that regulate actin-based motility processes in the nervous system. J Neurochem. 2002; 83:490–503. [PubMed: 12390511]
5. Luo L. Actin cytoskeleton regulation in neuronal morphogenesis and structural plasticity. Annu Rev Cell Dev Biol. 2002; 18:601–635. [PubMed: 12142283]
6. Rocca DL, Martin SP, Jenkins EL, Hanley JG. Inhibition of Arp2/3-mediated actin polymerization by PICK1 regulates neuronal morphology and AMPA receptor endocytosis. Nature Cell Biology. 2008; 10:259–271. [PubMed: 18297063]
7. Choi M, et al. Genetic diagnosis by whole exome capture and massively parallel DNA sequencing. Proc Natl Acad Sci USA. 2009; 106:19096–19101. [PubMed: 19861545]
8. DePristo MA, et al. A framework for variation discovery and genotyping using next-generation DNA sequencing data. Nature Genetics. 2011; 43:491–498. [PubMed: 21478889]
9. Magi A, et al. H3M2: detection of runs of homozygosity from whole-exome sequencing data. Bioinformatics. 2014; 30:2852–2859. [PubMed: 24966365]
10. Seelow D, Schuelke M, Hildebrandt F, Nurnberg P. HomozygosityMapper--an interactive approach to homozygosity mapping. Nucleic Acids Research. 2009; 37:W593–9. [PubMed: 19465395]
11. Ajioka I, Nakajima K. Switching of α-catenin from α-E-catenin in the cortical ventricular zone to α-N-catenin II in the intermediate zone. Developmental Brain Research. 2005; 160:106–111. [PubMed: 16185771]
12. Stocker AM, Chenn A. Differential expression of α-E-catenin and α-N-catenin in the developing cerebral cortex. Brain Research. 2006; 1073–1074:151–158.
13. Park C, Falls W, Finger JH, Longo-Guess CM, Ackerman SL. Deletion in Catna2, encoding αN-catenin, causes cerebellar and hippocampal lamination defects and impaired startle modulation. Nature Genetics. 2002; 31:279–284. [PubMed: 12089526]
14. Park C, Longo CM, Ackerman SL. Genetic and physical mapping of the cerebellar deficient folia (cdf) locus on mouse chromosome 6. Genomics. 2000; 69:135–138. [PubMed: 11013084]
15. Park C, Finger JH, Cooper JA, Ackerman SL. The cerebellar deficient folia (cdf) gene acts intrinsically in Purkinje cell migrations. genesis. 2002; 32:32–41. [PubMed: 11835672]
16. Togashi H, et al. Cadherin regulates dendritic spine morphogenesis. Neuron. 2002; 35:77–89. [PubMed: 12123610]
17. Abe K, Chisaka O, van Roy F, Takeichi M. Stability of dendritic spines and synaptic contacts is controlled by α-N-catenin. Nature Neuroscience. 2004; 7:357–363. [PubMed: 15034585]
18. Uemura M, Takeichi M. α-N-Catenin deficiency causes defects in axon migration and nuclear organization in restricted regions of the mouse brain. Dev Dyn. 2006; 235:2559–2566. [PubMed: 16691566]

19. Chambers SM, et al. Highly efficient neural conversion of human ES and iPS cells by dual inhibition of SMAD signaling. Nat Biotechnol. 2009; 27:275–280. [PubMed: 19252484]
20. Katakowski M, Zhang Z, deCarvalho AC, Chopp M. EphB2 induces proliferation and promotes a neuronal fate in adult subventricular neural precursor cells. Neurosci Lett. 2005; 385:204–209. [PubMed: 15970380]
21. Bershteyn M, et al. Human iPSC-derived cerebral organoids model cellular features of lissencephaly and reveal prolonged mitosis of outer radial glia. Stem Cell. 2017; 20:435–449.e4.
22. Torres M, et al. An α-E-catenin gene trap mutation defines its function in preimplantation development. PNAS. 1997; 94:901–906. [PubMed: 9023354]
23. Lein W-H, Klezovitch O, Fernandez TE, Delrow J, Vasioukhin V. αE-Catenin controls cerebral cortical size by regulating the hedgehog signaling pathway. Science. 2006:311. [PubMed: 16857929]
24. Pokutta S, Weis WI. Structure of the dimerization and β-catenin-binding region of α-catenin. Molecular Cell. 2000; 5:533–543. [PubMed: 10882138]
25. Hansen SD, et al. E-catenin actin-binding domain alters actin filament conformation and regulates binding of nucleation and disassembly factors. Molecular Biology of the Cell. 2013; 24:3710–3720. [PubMed: 24068324]
26. Wang P-S, et al. Crucial roles of the Arp2/3 complex during mammalian corticogenesis. Development (Cambridge, England). 2016
27. Rouiller I, et al. The structural basis of actin filament branching by the Arp2/3 complex. The Journal of Cell Biology. 2008; 180:887–895. [PubMed: 18316411]
28. Hetrick B, Han MS, Helgeson LA, Nolen BJ. Small molecules CK-666 and CK-869 inhibit actin-related protein 2/3 complex by blocking an activating conformational change. Chemistry & Biology. 2013; 20:701–712. [PubMed: 23623350]
29. Wynshaw-Boris A, Pramparo T, Youn YH, Hirotsune S. Lissencephaly: Mechanistic insights from animal models and potential therapeutic strategies. Semin Cell Dev Biol. 2010; 21:823–830. [PubMed: 20688183]
30. Moon HM, Wynshaw-Boris A. Cytoskeleton in action: lissencephaly, a neuronal migration disorder. Wiley Interdiscip Rev Dev Biol. 2013; 2:229–245. [PubMed: 23495356]
31. Solecki DJ, Model L, Gaetz J, Kapoor TM, Hatten ME. Par6α signaling controls glial-guided neuronal migration. Nature Neuroscience. 2004; 7:1195–1203. [PubMed: 15475953]
32. Strasser GA, Rahim NA, VanderWaal KE, Gertler FB, Lanier LM. Arp2/3 is a negative regulator of growth cone translocation. Neuron. 2004; 43:81–94. [PubMed: 15233919]
33. Kholmanskikh SS, Dobrin JS, Wynshaw-Boris A, Letourneau PC, Ross EM. Disregulated RhoGTPases and actin cytoskeleton contribute to the migration defect in Lis1-deficient neurons. The Journal of Neuroscience. 2003; 23:8673–8681. [PubMed: 14507966]
34. Chai X, Forster E, Zhao S, Bock HH, Frotscher M. Reelin stabilizes the actin cytoskeleton of neuronal processes by inducing n-cofilin phosphorylation at serine3. The Journal of Neuroscience. 2009; 29:288–299. [PubMed: 19129405]
35. Zhou FQ, Waterman-Storer CM, Cohan CS. Focal loss of actin bundles causes microtubule redistribution and growth cone turning. The Journal of Cell Biology. 2002; 157:839–849. [PubMed: 12034775]
36. Winkelman JD, et al. Fascin- and α-Actinin-bundled networks contain intrinsic structural features that drive protein sorting. Current Biology. 2016; 26:2697–2706. [PubMed: 27666967]
37. Hoffmann K, Lindner TH. easyLINKAGE-Plus--automated linkage analyses using large-scale SNP data. Bioinformatics. 2005; 21:3565–3567. [PubMed: 16014370]
38. Lardelli RM, et al. Bi-allelic mutations in the 3′ exonuclease TOE1 cause pontocerebellar hypoplasia and uncover a role in snRNA processing. Nature Genetics. 2017; 49:457–464. [PubMed: 28092684]
39. Okita K, et al. A more efficient method to generate integration-free human iPS cells. Nature Methods. 2011; 8:409–412. [PubMed: 21460823]
40. Marchetto MCN, et al. A model for neural development and treatment of Rett syndrome using human induced pluripotent stem cells. Cell. 2010; 143:527–539. [PubMed: 21074045]

41. Ran FA, et al. Genome engineering using the CRISPR-Cas9 system. Nat Protoc. 2013; 8:2281–2308. [PubMed: 24157548]

42. Youn YH, Pramparo T, Hirotsune S, Wynshaw-Boris A. Distinct dose-dependent cortical neuronal migration and neurite extension defects in Lis1 and Ndel1 mutant mice. The Journal of Neuroscience. 2009; 29:15520–15530. [PubMed: 20007476]

43. Yeung YG, Wang Y, Einstein DB, Lee PS, Stanley ER. Colony-stimulating factor-1 stimulates the formation of multimeric cytosolic complexes of signaling proteins and cytoskeletal components in macrophages. J Biol Chem. 1998; 273:17128–17137. [PubMed: 9642280]

44. Gleeson JG, Lin PT, Flanagan LA, Walsh CA. Doublecortin is a microtubule-associated protein and is expressed widely by migrating neurons. Neuron. 1999; 23:257–271. [PubMed: 10399933]

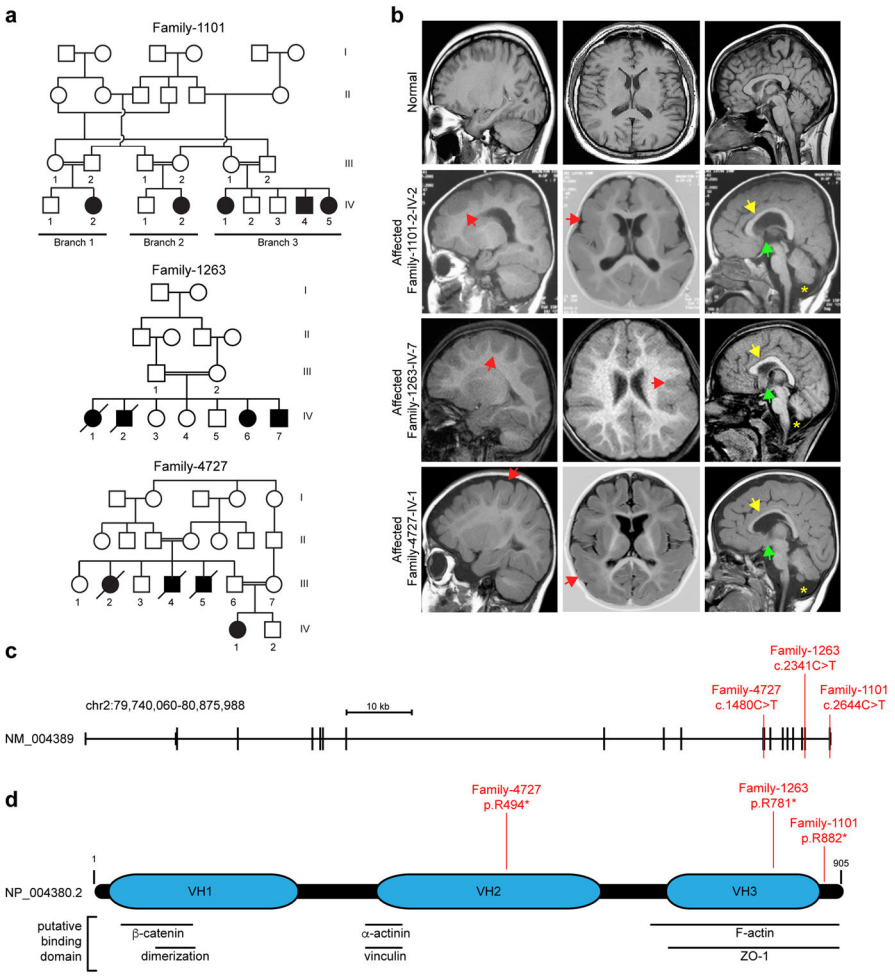

Figure 1. Identification of homozygous truncating *CTNNA2* mutations in families with pachygyria

(a) Pedigrees of three consanguineous families. Parental consanguinity: double bar. Asterisk: sampled individual, Square: male, Circle: female, Filled: affected.

(b) Sagittal, axial, and midline sagittal MRI with symmetrically thickened cortex (red arrowheads) and paucity of cortical gyri, consistent with pachygyria. Patents present with thin corpus callosum (yellow arrowheads), absent anterior commissure (green arrowheads), and fluid cavity as a result of cerebellar hypoplasia (mega cisterna magna, yellow asterisk).

(c) *CTNNA2* genomic organization, and location of mutations in Families 1101, 1263 and 4727 in red.

(d) CTNNA2 905 aa polypeptide (Entrez NP_004380.2) with Vinculin Homology domains (VH1-3), and putative protein binding sites. Patient homozygous truncating mutations in red.

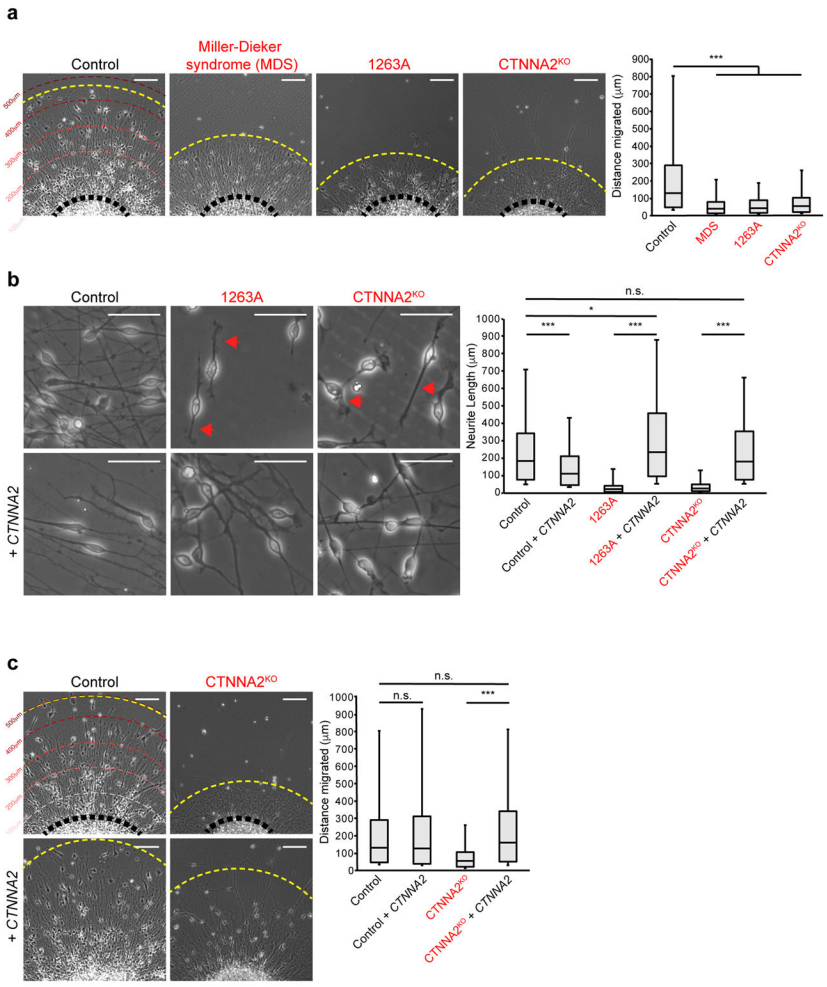

Figure 2. Loss of *CTNNA2* mirrors Miller-Dieker syndrome (MDS) migration phenotypes in iPSC-derived neurons

(a) Quantification of neuronal migration from human iPSC-derived neurospheres. MDS-derived neurons do not migrate as far as Control neurons. Migrating neurons from affected member of Family-1263 (1263A) showed reduced migration, similar to *CTNNA2*^{KO} neurons. The distribution of migrating neurons at right, box plot with top box: Q3, bottom box: Q1, and Median. The whiskers represent the minimum and maximum values observed in the dataset. Repeated in three independent iPSC clones per patient or three *CTNNA2*^{KO} clones, 828 cells scored. *, significance (see Statistics and Reproducibility) Scale bar 100 μm.

(b) Control neurons show bipolar morphology with long extended primary neurites. *CTNNA2* patient and knockout neurons show thickened, short neurites (red arrows), rescued by forced expression of *CTNNA2*. The distribution of neurite length at right, box plot with top box: Q3, bottom box: Q1, and Median displayed. The whiskers represent the minimum and maximum values observed in the dataset. Repeated in three independent iPSC clones per patient or three *CTNNA2*^{KO} clones, 552 cells scored. *, significance (see Statistics and Reproducibility). Scale bar 50 μm.

(c) Rescue of neuronal cell body migration distance upon forced expression of *CTNNA2* in $CTNNA2^{KO}$ lines. The distribution of migrating neurons at right, box plot with top box: Q3, bottom box: Q1, and Median displayed. The whiskers represent the minimum and maximum values observed in the dataset. Repeated in three $CTNNA2^{KO}$ clones, 532 cells scored. * and ***, significant *P* (see Statistics and Reproducibility). Scale bar 100 μm.

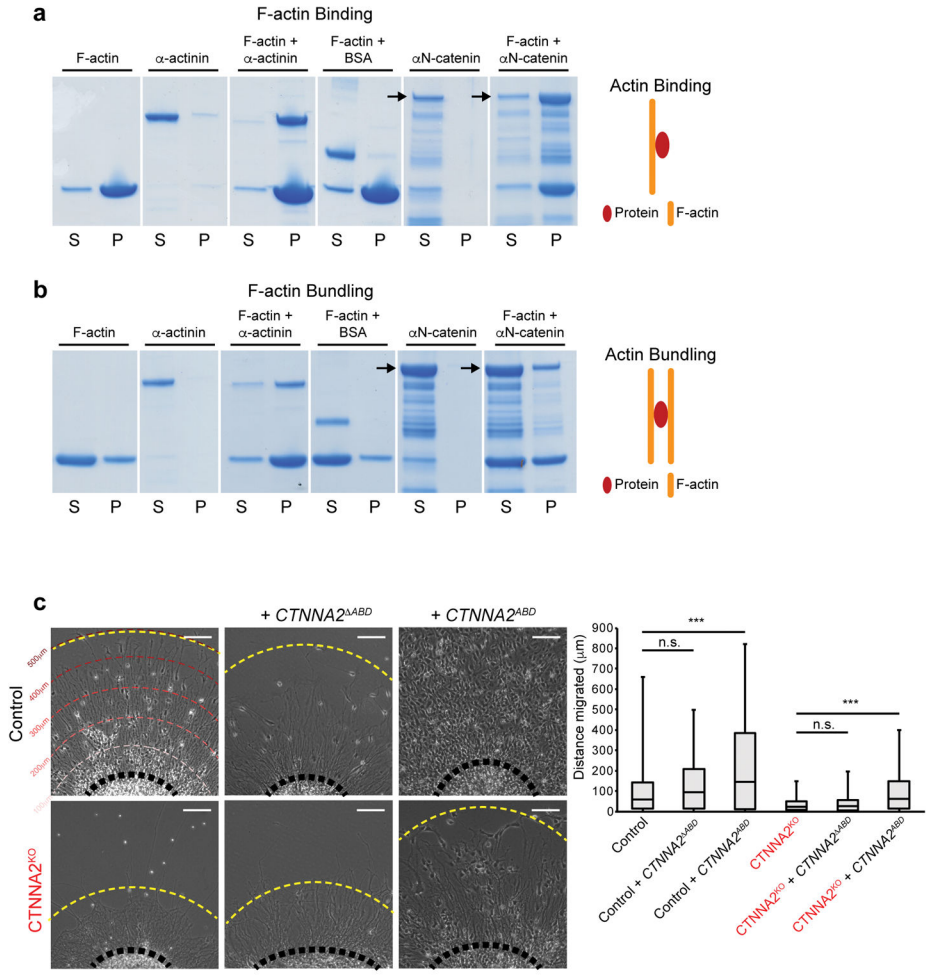

Figure 3. Recombinant αN-catenin associates with F-actin, and the actin-binding domain is necessary and sufficient for rescue of neuronal migration

(a) αN-catenin binds to F-actin in co-sedimentation assays. The majority of F-actin was present in the pellet (P) upon 100,000g spin, and while α-actinin was observed primarily in the supernatant (S) when centrifuged alone, when sedimented with F-actin shifted to P. BSA was found in S even when sedimented with F-actin. αN-catenin was exclusively in S when centrifuged alone, but when sedimented with F-actin the full-length band shifted to P. Repeated in duplicate.

(b) αN-catenin weakly promotes bundling of F-actin in an assembly assay. Upon centrifugation at 10,000g, F-actin was split between S and P. While α-actinin was exclusively in S, when co-pelleted with F-actin promoted a shift of actin to P. BSA showed no bundling activity. Similar to α-actinin, αN-catenin was exclusively in S, but promoted a slight shift of actin to P. Repeated in duplicate.

(c) Migration assay showing rescue of neuronal migration upon forced lentiviral expression of the actin-binding domain of αN-catenin (*CTNNA2*^{ABD}) but not αN-catenin lacking the actin-binding domain (*CTNNA2*$^{\Delta ABD}$). Quantification shown at right, box plot with top box: Q3, bottom box: Q1, and Median displayed. The whiskers represent the minimum and

maximum values observed in the dataset. Repeated in three *CTNNA2*^{KO} clones, 834 cells scored. ***, significant *P* (see Statistics and Reproducibility). Scale bar 100 μm.

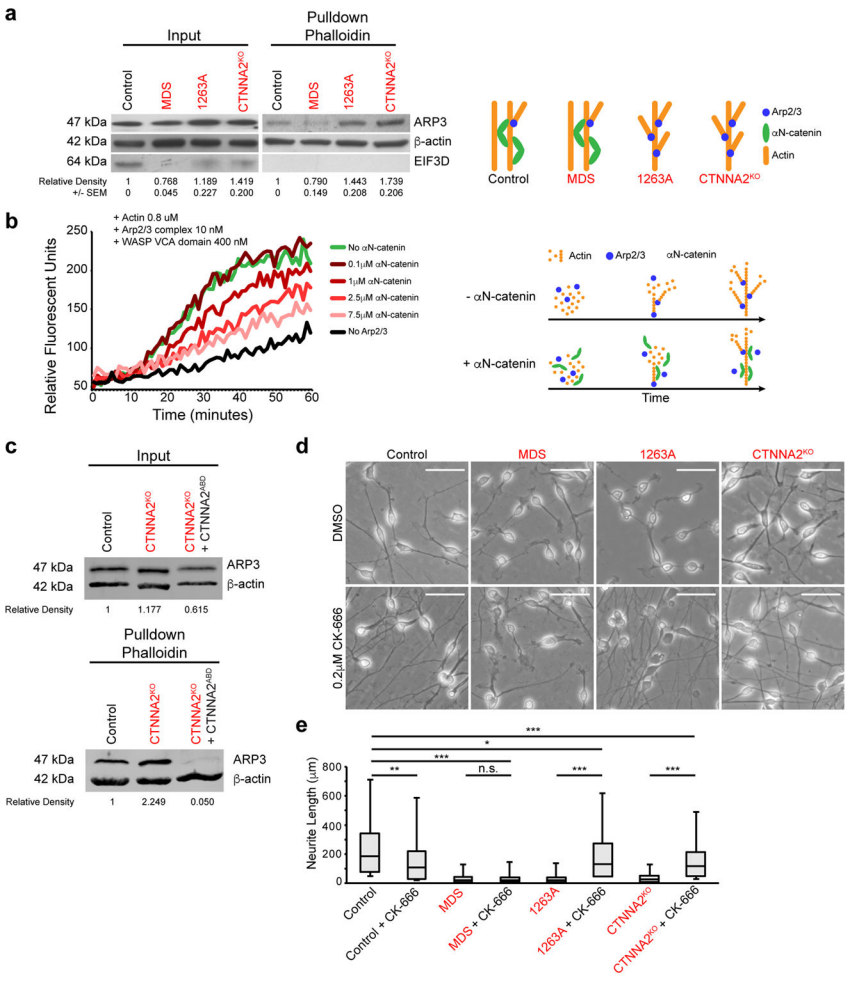

Figure 4. αN-catenin represses Arp2/3-actin association and polymerization

(a) Elevated association between affinity-purified F-actin and ARP2/3 in *CTNNA2*-mutant cells. Input: basal expression. F-actin pulldown with phalloidin. Exaggerated ARP3 band in 1263A and knockout lines, compared MDS or Control line. EIF3D (does not bind actin) as a control for pulldown specificity. Cropped images shown. Repeated in triplicate, quantification and SEM below. Schematic depicts model (right).

(b) Actin polymerization assay showing dose-dependent inhibition of Arp2/3 + VCA domain of WASP mediated actin polymerization by αN-catenin, measured by relative fluorescent units. In the absence of Arp2/3 (black) there was minimal polymerization, but when Arp2/3 + VCA was added (green) polymerization increased substantially, which was reversed upon dose escalation of αN-catenin. Repeated in triplicate. Schematic depicts model (right).

(c) Loss of association between F-actin and ARP2/3 in *CTNNA2*^{KO} cells expressing the actin binding domain (ABD) of αN-catenin. Input: basal expression of ARP3 and Actin. F-actin pulldown with phalloidin. Exaggerated ARP3 band in knockout neurons, and loss of ARP3 in ABD-expressing knockout neurons, compared with band in Control line. Quantification by relative fluorescence of ARP3 to Actin. Cropped images shown. Repeated in duplicate.

(d) ARP2/3 inhibition by CK-666 rescued neurite length defect in *CTNNA2* mutant neurons, but not Control and MDS mutant neurons. Scale bar 50 μm.
(e) Quantification of (d) with top and bottom quartiles and Median displayed. Whiskers represent the minimum and maximum values observed in the dataset. Repeated in three independent iPSC clones per patient or three $CTNNA2^{KO}$ clones, 442 cells scored.*, ** and ***, significant *P* (see Statistics and Reproducibility).

Table 1

Clinical Phenotypes

Patients display acquired microcephaly, hypotonic cerebral palsy, inability to ambulate or speak, and intractable seizures. HC, head circumference; SD, standard deviation below the mean; B/L, bi-lateral; VEP, visual evoked potential; ERG, electroretinogram; EEG, electroencephalogram.

	Family-1101-1-IV-2	**Family 1101-2-IV-2**	**Family-1101-3-IV-1**	**Family-1101-3-IV-4**	**Family-1263-1**	**Family-1263-2**	**Family-4727-IV-1**
Gender	F	F	F	M	M	F	F
Origin	Saudi	Saudi	Saudi	Saudi	Turkish	Turkish	Saudi
Weight at birth (kg)	2.9	N/A	N/A	N/A	2.7	2.5	3.5
Length at birth (cm)	46	N/A	N/A	N/A	49	48	N/A
HC at birth (cm)	35.5	N/A	N/A	N/A	N/A	N/A	N/A
HC at birth (SD)	0	N/A	N/A	N/A	N/A	N/A	N/A
HC at last examination (cm)	50	53.5	53	51	44	47	46.5
HC at last examination (SD)	−4	−1/0	−1	−2/−1	−5	−5	−5
Diagnosis age	2 yrs	1.5 yrs	1 yr	Birth	30 mos	9 yrs	28 mos
Intellectual Disability	Severe	Severe	Severe	Severe	Severe	Severe	N/A
Development							
Gross motor (normal/delayed/absent)	Delayed	Delayed	Delayed	Delayed	Delayed	Absent	Delayed
Fine motor (normal/delayed/absent)	Delayed	Delayed	Delayed	Delayed	Delayed	Absent	Delayed
Language (normal/delayed/absent)	Single words	Single words	Single words	Absent	Absent	Absent	Absent
Social (normal/delayed/absent)	Delayed	Delayed	Delayed	Delayed	Delayed	Absent	Delayed
Seizures							
Onset	2–3 yrs	1.5 yrs	6 mos	3 yrs	8 mos	6 mos	6 mos
Type	Variable-atonic	Atonic/myoclonic	Variable-atonic	Variable-atonic	Atonic/myoclonic	Atonic/myoclonic	Infantile spasm (hypsarrhythmia)
Frequency	1–2/week	1–2/week	1–2/week	1–2/week	monthly	monthly	N/A
Neurological Findings							
Hypertonia	−	−	−	−	−	−	+
Hypotonia	+	+	−	+	+	+	+ (truncal)
Deep tendon reflexes	Increased	Increased	−	Increased	Increased	Increased	Increased
Spastic tetraplegia	+	−	−	+	−	+	+
Ataxia	Nonambulatory	+	+	Nonambulatory	−	Nonambulatory	Nonambulatory

	Family-1101-1-IV-2	Family 1101-2-IV-2	Family-1101-3-IV-1	Family-1101-3-IV-4	Family-1263-1	Family-1263-2	Family-4727-IV-1
Investigations							
Metabolic	Normal	Normal	Normal	Normal	N/A	N/A	Negative
VEP/ERG	Normal	Normal	N/A	Abnormal	N/A	N/A	N/A
EEG	Abnormal	Abnormal	Abnormal	Abnormal	Abnormal	Abnormal	Abnormal
MRI							
Lissencephaly spectrum	Pachygyria	Pachygyria	Pachygyria	Pachygyria	Pachygyria	Pachygyria	Pachygyria
Cerebral mantle thickening (normal 5 mm)	9–30mm	12–35mm	10–30mm	10–32mm	12–22mm	9–24mm	9–35mm
Subcortical band heterotopia	–	–	–	–	–	–	–
Corpus callosum	N/A	N/A	thin	thin	thin	thin	thin
Cerebellar hypoplasia	Y	Y	Y	Y	Y	Y	Y
Brainstem hypoplasia	N	N	N	N	N	N	Y
Hydrocephalus	N	N	N	N	N	N/A	N/A
White matter paucity	Y	Y	Y	Y	Y	Y	N/A
White matter signal	N/A	N/A	N/A	N/A	N/A	N/A	N/A
Miscellaneous							
Polyhydrammios	–	–	–	–	–	–	–
Lung hypoplasia	–	–	–	–	–	–	–
Short stature	–	–	–	–	–	–	–
Macrocephaly	–	–	–	–	–	–	–
Optic atrophy	–	–	–	–	–	–	–
Autistic features	+	+	+	+	+	+	+
Dysmorphism	–	–	–	–	B/L pes equinovarus	–	–